

Hadronization geometry and charge-dependent two-particle correlations on momentum subspace (η, ϕ) in Au-Au collisions at $\sqrt{s_{NN}} = 130$ GeV

- J. Adams,³ M.M. Aggarwal,²⁹ Z. Ahammed,⁴³ J. Amonett,²⁰ B.D. Anderson,²⁰ D. Arkhipkin,¹³ G.S. Averichev,¹² S.K. Badyal,¹⁹ Y. Bai,²⁷ J. Balewski,¹⁷ O. Barannikova,³² L.S. Barnby,³ J. Baudot,¹⁸ S. Bekele,²⁸ V.V. Belaga,¹² R. Bellwied,⁴⁶ J. Berger,¹⁴ B.I. Bezverkhny,⁴⁸ S. Bharadwaj,³³ A. Bhasin,¹⁹ A.K. Bhati,²⁹ V.S. Bhatia,²⁹ H. Bichsel,⁴⁵ A. Billmeier,⁴⁶ L.C. Bland,⁴ C.O. Blyth,³ B.E. Bonner,³⁴ M. Botje,²⁷ A. Boucham,³⁸ A.V. Brandin,²⁵ A. Bravar,⁴ M. Bystersky,¹¹ R.V. Cadman,¹ X.Z. Cai,³⁷ H. Caines,⁴⁸ M. Calderón de la Barca Sánchez,⁴ J. Carroll,²¹ J. Castillo,²¹ D. Cebra,⁷ Z. Chajecski,⁴⁴ P. Chaloupka,¹¹ S. Chattopdhyay,⁴³ H.F. Chen,³⁶ Y. Chen,⁸ J. Cheng,⁴¹ M. Cherney,¹⁰ A. Chikanian,⁴⁸ W. Christie,⁴ J.P. Coffin,¹⁸ T.M. Cormier,⁴⁶ J.G. Cramer,⁴⁵ H.J. Crawford,⁶ D. Das,⁴³ S. Das,⁴³ M.M. de Moura,³⁵ A.A. Derevschikov,³¹ L. Didenko,⁴ T. Dietel,¹⁴ S.M. Dogra,¹⁹ W.J. Dong,⁸ X. Dong,³⁶ J.E. Draper,⁷ F. Du,⁴⁸ A.K. Dubey,¹⁵ V.B. Dunin,¹² J.C. Dunlop,⁴ M.R. Dutta Mazumdar,⁴³ V. Eckardt,²³ W.R. Edwards,²¹ L.G. Efimov,¹² V. Emelianov,²⁵ J. Engelage,⁶ G. Eppley,³⁴ B. Erazmus,³⁸ M. Estienne,³⁸ P. Fachini,⁴ J. Faivre,¹⁸ R. Fatemi,¹⁷ J. Fedorisin,¹² K. Filimonov,²¹ P. Filip,¹¹ E. Finch,⁴⁸ V. Fine,⁴ Y. Fisyak,⁴ K.J. Foley,⁴ K. Fomenko,¹² J. Fu,⁴¹ C.A. Gagliardi,³⁹ J. Gans,⁴⁸ M.S. Ganti,⁴³ L. Gaudichet,³⁸ F. Geurts,³⁴ V. Ghazikhanian,⁸ P. Ghosh,⁴³ J.E. Gonzalez,⁸ O. Grachov,⁴⁶ O. Grebenyuk,²⁷ D. Grosnick,⁴² S.M. Guertin,⁸ Y. Guo,⁴⁶ A. Gupta,¹⁹ T.D. Gutierrez,⁷ T.J. Hallman,⁴ A. Hamed,⁴⁶ D. Hardtke,²¹ J.W. Harris,⁴⁸ M. Heinz,² T.W. Henry,³⁹ S. Hepplemann,³⁰ B. Hippolyte,⁴⁸ A. Hirsch,³² E. Hjort,²¹ G.W. Hoffmann,⁴⁰ H.Z. Huang,⁸ S.L. Huang,³⁶ E.W. Hughes,⁵ T.J. Humanic,²⁸ G. Igo,⁸ A. Ishihara,⁴⁰ P. Jacobs,²¹ W.W. Jacobs,¹⁷ M. Janik,⁴⁴ H. Jiang,⁸ P.G. Jones,³ E.G. Judd,⁶ S. Kabana,² K. Kang,⁴¹ M. Kaplan,⁹ D. Keane,²⁰ V.Yu. Khodyrev,³¹ J. Kiryluk,²² A. Kisiel,⁴⁴ E.M. Kislov,¹² J. Klay,²¹ S.R. Klein,²¹ A. Klyachko,¹⁷ D.D. Koetke,⁴² T. Kollegger,¹⁴ M. Kopytine,²⁰ L. Kotchenda,²⁵ M. Kramer,²⁶ P. Kravtsov,²⁵ V.I. Kravtsov,³¹ K. Krueger,¹ C. Kuhn,¹⁸ A.I. Kulikov,¹² A. Kumar,²⁹ C.L. Kunz,⁹ R.Kh. Kutuev,¹³ A.A. Kuznetsov,¹² M.A.C. Lamont,⁴⁸ J.M. Landgraf,⁴ S. Lange,¹⁴ F. Laue,⁴ J. Lauret,⁴ A. Lebedev,⁴ R. Lednicky,¹² S. Lehocka,¹² M.J. LeVine,⁴ C. Li,³⁶ Q. Li,⁴⁶ Y. Li,⁴¹ S.J. Lindenbaum,²⁶ M.A. Lisa,²⁸ F. Liu,⁴⁷ L. Liu,⁴⁷ Q.J. Liu,⁴⁵ Z. Liu,⁴⁷ T. Ljubicic,⁴ W.J. Llope,³⁴ H. Long,⁸ R.S. Longacre,⁴ M. Lopez-Noriega,²⁸ W.A. Love,⁴ Y. Lu,⁴⁷ T. Ludlam,⁴ D. Lynn,⁴ G.L. Ma,³⁷ J.G. Ma,⁸ Y.G. Ma,³⁷ D. Magestro,²⁸ S. Mahajan,¹⁹ D.P. Mahapatra,¹⁵ R. Majka,⁴⁸ L.K. Mangotra,¹⁹ R. Manweiler,⁴² S. Margetis,²⁰ C. Markert,⁴⁸ L. Martin,³⁸ J.N. Marx,²¹ H.S. Matis,²¹ Yu.A. Matulenko,³¹ C.J. McClain,¹ T.S. McShane,¹⁰ F. Meissner,²¹ Yu. Melnick,³¹ A. Meschanin,³¹ M.L. Miller,²² Z. Milosevich,⁹ N.G. Minaev,³¹ C. Mironov,²⁰ A. Mischke,²⁷ D.K. Mishra,¹⁵ J. Mitchell,³⁴ B. Mohanty,⁴³ L. Molnar,³² C.F. Moore,⁴⁰ D.A. Morozov,³¹ M.G. Munhoz,³⁵ B.K. Nandi,⁴³ S.K. Nayak,¹⁹ T.K. Nayak,⁴³ J.M. Nelson,³ P.K. Netrakanti,⁴³ V.A. Nikitin,¹³ L.V. Nogach,³¹ S.B. Nurushev,³¹ G. Odyniec,²¹ A. Ogawa,⁴ V. Okorokov,²⁵ M. Oldenburg,²¹ D. Olson,²¹ S.K. Pal,⁴³ Y. Panebratsev,¹² S.Y. Panitkin,⁴ A.I. Pavlinov,⁴⁶ T. Pawlak,⁴⁴ T. Peitzmann,²⁷ V. Perevoztchikov,⁴ C. Perkins,⁶ W. Peryt,⁴⁴ V.A. Petrov,¹³ S.C. Phatak,¹⁵ R. Picha,⁷ M. Planinic,⁴⁹ J. Pluta,⁴⁴ N. Porile,³² J. Porter,⁴⁵ A.M. Poskanzer,²¹ M. Potekhin,⁴ E. Potrebenikova,¹² B.V.K.S. Potukuchi,¹⁹ D. Prindle,⁴⁵ C. Pruneau,⁴⁶ J. Putschke,²³ G. Rai,²¹ G. Rakness,³⁰ R. Raniwala,³³ S. Raniwala,³³ O. Ravel,³⁸ R.L. Ray,⁴⁰ S.V. Razin,¹² D. Reichhold,³² J.G. Reid,⁴⁵ G. Renault,³⁸ F. Retiere,²¹ A. Ridiger,²⁵ H.G. Ritter,²¹ J.B. Roberts,³⁴ O.V. Rogachevskiy,¹² J.L. Romero,⁷ A. Rose,⁴⁶ C. Roy,³⁸ L. Ruan,³⁶ R. Sahoo,¹⁵ I. Sakrejda,²¹ S. Salur,⁴⁸ J. Sandweiss,⁴⁸ I. Savin,¹³ P.S. Sazhin,¹² J. Schambach,⁴⁰ R.P. Scharenberg,³² N. Schmitz,²³ L.S. Schroeder,²¹ K. Schweda,²¹ J. Seger,¹⁰ P. Seyboth,²³ E. Shahaliev,¹² M. Shao,³⁶ W. Shao,⁵ M. Sharma,²⁹ W.Q. Shen,³⁷ K.E. Shestermanov,³¹ S.S. Shimanskiy,¹² E. Sichtermann,²¹ F. Simon,²³ R.N. Singaraju,⁴³ G. Skoro,¹² N. Smirnov,⁴⁸ R. Snellings,²⁷ G. Sood,⁴² P. Sorensen,²¹ J. Sowinski,¹⁷ J. Speltz,¹⁸ H.M. Spinka,¹ B. Srivastava,³² A. Stadnik,¹² T.D.S. Stanislaus,⁴² R. Stock,¹⁴ A. Stolpovsky,⁴⁶ M. Strikhanov,²⁵ B. Stringfellow,³² A.A.P. Suaide,³⁵ E. Sugarbaker,²⁸ C. Suire,⁴ M. Sumbera,¹¹ B. Surrow,²² T.J.M. Symons,²¹ A. Szanto de Toledo,³⁵ P. Szarwas,⁴⁴ A. Tai,⁸ J. Takahashi,³⁵ A.H. Tang,²⁷ T. Tarnowsky,³² D. Thein,⁸ J.H. Thomas,²¹ S. Timoshenko,²⁵ M. Tokarev,¹² T.A. Trainor,⁴⁵ S. Trentalange,⁸ R.E. Tribble,³⁹ O.D. Tsai,⁸ J. Ulery,³² T. Ullrich,⁴ D.G. Underwood,¹ A. Urkinbaev,¹² G. Van Buren,⁴ M. van Leeuwen,²¹ A.M. Vander Molen,²⁴ R. Varma,¹⁶ I.M. Vasilevski,¹³ A.N. Vasiliev,³¹ R. Vernet,¹⁸ S.E. Vigdor,¹⁷ V.P. Viyogi,⁴³ S. Vokal,¹² S.A. Voloshin,⁴⁶ M. Vznuzdaev,²⁵ W.T. Wagoner,¹⁰ F. Wang,³² G. Wang,²⁰ G. Wang,⁵ X.L. Wang,³⁶ Y. Wang,⁴⁰ Y. Wang,⁴¹ Z.M. Wang,³⁶ H. Ward,⁴⁰ J.W. Watson,²⁰ J.C. Webb,¹⁷ R. Wells,²⁸ G.D. Westfall,²⁴ A. Wetzler,²¹ C. Whitten Jr.,⁸ H. Wieman,²¹ S.W. Wissink,¹⁷ R. Witt,² J. Wood,⁸ J. Wu,³⁶ N. Xu,²¹ Z. Xu,⁴ Z.Z. Xu,³⁶ E. Yamamoto,²¹ P. Yepes,³⁴ V.I. Yurevich,¹² Y.V. Zanevsky,¹² H. Zhang,⁴ W.M. Zhang,²⁰ Z.P. Zhang,³⁶ P.A. Zolnierczuk,¹⁷ R. Zoulkarneev,¹³ Y. Zoulkarneeva,¹³ and A.N. Zubarev¹²

(STAR Collaboration)

- ¹Argonne National Laboratory, Argonne, Illinois 60439
²University of Bern, 3012 Bern, Switzerland
³University of Birmingham, Birmingham, United Kingdom
⁴Brookhaven National Laboratory, Upton, New York 11973
⁵California Institute of Technology, Pasadena, California 91125
⁶University of California, Berkeley, California 94720
⁷University of California, Davis, California 95616
⁸University of California, Los Angeles, California 90095
⁹Carnegie Mellon University, Pittsburgh, Pennsylvania 15213
¹⁰Creighton University, Omaha, Nebraska 68178
¹¹Nuclear Physics Institute AS CR, 250 68 Řež/Prague, Czech Republic
¹²Laboratory for High Energy (JINR), Dubna, Russia
¹³Particle Physics Laboratory (JINR), Dubna, Russia
¹⁴University of Frankfurt, Frankfurt, Germany
¹⁵Institute of Physics, Bhubaneswar 751005, India
¹⁶Indian Institute of Technology, Mumbai, India
¹⁷Indiana University, Bloomington, Indiana 47408
¹⁸Institut de Recherches Subatomiques, Strasbourg, France
¹⁹University of Jammu, Jammu 180001, India
²⁰Kent State University, Kent, Ohio 44242
²¹Lawrence Berkeley National Laboratory, Berkeley, California 94720
²²Massachusetts Institute of Technology, Cambridge, MA 02139-4307
²³Max-Planck-Institut für Physik, Munich, Germany
²⁴Michigan State University, East Lansing, Michigan 48824
²⁵Moscow Engineering Physics Institute, Moscow Russia
²⁶City College of New York, New York City, New York 10031
²⁷NIKHEF, Amsterdam, The Netherlands
²⁸Ohio State University, Columbus, Ohio 43210
²⁹Panjab University, Chandigarh 160014, India
³⁰Pennsylvania State University, University Park, Pennsylvania 16802
³¹Institute of High Energy Physics, Protvino, Russia
³²Purdue University, West Lafayette, Indiana 47907
³³University of Rajasthan, Jaipur 302004, India
³⁴Rice University, Houston, Texas 77251
³⁵Universidade de Sao Paulo, Sao Paulo, Brazil
³⁶University of Science & Technology of China, Anhui 230027, China
³⁷Shanghai Institute of Applied Physics, Shanghai 201800, China
³⁸SUBATECH, Nantes, France
³⁹Texas A&M University, College Station, Texas 77843
⁴⁰University of Texas, Austin, Texas 78712
⁴¹Tsinghua University, Beijing 100084, China
⁴²Valparaiso University, Valparaiso, Indiana 46383
⁴³Variable Energy Cyclotron Centre, Kolkata 700064, India
⁴⁴Warsaw University of Technology, Warsaw, Poland
⁴⁵University of Washington, Seattle, Washington 98195
⁴⁶Wayne State University, Detroit, Michigan 48201
⁴⁷Institute of Particle Physics, CCNU (HZNU), Wuhan 430079, China
⁴⁸Yale University, New Haven, Connecticut 06520
⁴⁹University of Zagreb, Zagreb, HR-10002, Croatia

(Dated: September 23, 2004)

We present the first measurements of charge-dependent two-particle correlations on momentum-space difference variables $\eta_1 - \eta_2$ (pseudorapidity) and $\phi_1 - \phi_2$ (azimuth) for primary charged hadrons with transverse momentum $0.15 \leq p_t \leq 2$ GeV/c and $|\eta| \leq 1.3$ from Au-Au collisions at $\sqrt{s_{NN}} = 130$ GeV. We observe correlation structures not predicted by theory but consistent with evolution of hadron emission geometry with increasing centrality from one-dimensional fragmentation of color strings to higher-dimensional fragmentation of a hadron-opaque bulk medium.

PACS numbers: 24.60.Ky, 25.75.Gz

The analysis of correlations and fluctuations plays an important role in studies of the colored medium pro-

duced in ultrarelativistic heavy ion collisions [1, 2, 3]. Specifically, *in-medium modification* of color-string frag-

mentation and hard parton scattering in heavy ion collisions affects large-momentum-scale two-particle correlations (momentum difference comparable to the STAR detector acceptance). Large-scale correlations may result from initial-state multiple scattering [4, 5], in-medium dissipation [6] and fragmentation of the colored medium to final-state hadrons (fragmentation of strings in p-p, fragmentation of the bulk medium in A-A). String fragmentation models [7] describe correlations on (η, ϕ) in high-energy p-p collisions in terms of local conservation of transverse momentum and net charge (canonical suppression of net-momentum and net-charge fluctuations). The corresponding process in A-A collisions is an open question. Predictions have been made of dramatic suppression of net-charge fluctuations in central A-A collisions as signaling quark-gluon plasma formation [8].

In this Letter we report the first measurement in heavy ion collisions of the centrality dependence of two-particle *charge-dependent* correlations (like – unlike sign charge-pairs) distributed on *difference variables* $\phi_\Delta \equiv \phi_1 - \phi_2$ and $\eta_\Delta \equiv \eta_1 - \eta_2$. The data suggest that local charge conservation at hadronization plus increasing system density and spatial extent result in evolution with Au-Au centrality from one-dimensional (1D) *charge-ordering* (locally-alternating charge signs) on configuration space z (beam axis) to two-dimensional (2D) charge ordering on (z, ϕ) . Those results were not anticipated by theoretical models [5, 9]. This analysis is based on Au-Au collisions at $\sqrt{s_{NN}} = 130$ GeV obtained with the STAR detector at the Relativistic Heavy Ion Collider (RHIC).

Charge-dependent (CD) number-density *autocorrelation* distributions on difference variables [10] access the *charge-dependent* structure of two-particle density $\rho(\vec{p}_1, \vec{p}_2)$, projected in this analysis onto momentum components $(\eta_1, \eta_2, \phi_1, \phi_2)$. Differential correlation analysis is achieved by comparing object and reference distributions, the former comprised of particle pairs formed from single events (sibling pairs), the latter of pairs formed from different but similar events (mixed pairs). The two-particle correlation function and pair-number density ratio distribution are then defined respectively by

$$\begin{aligned} C(\vec{p}_1, \vec{p}_2) &= \rho_{mix}(\vec{p}_1, \vec{p}_2) [r(\vec{p}_1, \vec{p}_2) - 1], \\ r(\vec{p}_1, \vec{p}_2) &= \rho_{sib}(\vec{p}_1, \vec{p}_2) / \rho_{mix}(\vec{p}_1, \vec{p}_2). \end{aligned} \quad (1)$$

In this analysis, pair-number densities $\rho(a, b; \vec{p}_1, \vec{p}_2)$ for charge-pair combinations ($a = \pm, b = \pm$) were projected onto variable pairs (η_1, η_2) , (ϕ_1, ϕ_2) and difference variables $(\eta_\Delta, \phi_\Delta)$ as histograms of pair numbers $n_{ab,ij} \simeq \epsilon_x \epsilon_y \rho(a, b; x_i, y_j)$, where ϵ_x, ϵ_y are bin widths on variables $x, y \in \{\eta, \phi, \eta_\Delta, \phi_\Delta\}$. Sibling and mixed pair numbers for each charge-pair type were separately normalized to the total number of detected pairs in each event class: $\hat{n}_{ab,ij} = n_{ab,ij} / \sum_{ij} n_{ab,ij}$. Normalized pair-number ratios $\hat{r}_{ab,ij} = \hat{n}_{ab,ij,sib} / \hat{n}_{ab,ij,mix}$ are the basis for this analysis. To reduce systematic error, ratio histograms were obtained for subsets of events with similar centralities (multiplicities differ by ≤ 50) and primary-vertex location (within 7.5 cm along the beam axis). Ra-

tios $\hat{r}_{ab,ij}$ for each centrality were defined as weighted averages over all subsets in that centrality class. Ratios were further combined to form like-sign (LS: $a = b$), unlike-sign (US: $a \neq b$), and charge-dependent (CD = LS – US) ratios (the last definition compatible with isospin convention and net-charge fluctuation measures) [11].

Data for this analysis were obtained with the STAR detector [12] using a 0.25 T uniform magnetic field parallel to the beam axis. A minimum-bias event sample required coincidence of two Zero-Degree Calorimeters (ZDC); a 0-15% of total cross section event sample was defined by a threshold on the Central Trigger Barrel (CTB), with ZDC coincidence. Event triggering and charged-particle measurements with the Time Projection Chamber (TPC) are described in [12]. Tracking efficiencies, event and track quality cuts and primary-particle definition are described in [11, 13]. Tracks were accepted in $|\eta| \leq 1.3$, full azimuth and $0.15 \leq p_t \leq 2$ GeV/c. Particle identification was not implemented. Corrections were made to ratio \hat{r} for two-track inefficiencies due to track splitting and merging. Small-scale structures due to quantum, Coulomb and strong-interaction correlations [14] were suppressed by eliminating sibling *and* mixed track pairs ($\sim 22\%$ of total) with $|\eta_\Delta| < 1.0$, $|\phi_\Delta| < 1.0$ and $|p_{t1} - p_{t2}| < 0.2$ GeV/c if $p_t < 0.8$ GeV/c for either particle. Those cuts do not significantly affect structures in Fig. 2. Four centrality classes for 300k events labeled (a) - (d) for central to peripheral were defined [15] by cuts on TPC track multiplicity N within the acceptance relative to end-point multiplicity N_0 , which corresponds to the maximum participant number [11, 16].

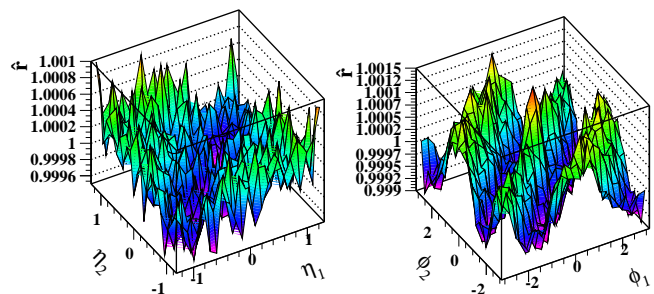


FIG. 1: Normalized LS pair-number ratios \hat{r} for collisions in centrality class (a) (most central) for (η_1, η_2) (left panel) and (ϕ_1, ϕ_2) (right panel).

Fig. 1 shows ratio \hat{r} for the LS charge combination on (η_1, η_2) and (ϕ_1, ϕ_2) for centrality class (a). Deviations from unity, $\hat{r} - 1$, of this *per-pair* variable contain a trivial *dilution factor* $1/\bar{N}$ (\bar{N} is the mean multiplicity in the acceptance) and are therefore typically a few *permil* for central Au-Au collisions. However, the correlations remain highly significant compared to statistical errors (*cf.* Figs. 2-4). Quadrupole or v_2 structures (associated with elliptic flow) plus additional same-side ($|\phi_\Delta| < \pi/2$) structure dominate the right panel. The *anticorrelated* LS distribution on η_Δ in the left panel is suggestive of charge ordering from string fragmentation in p-p colli-

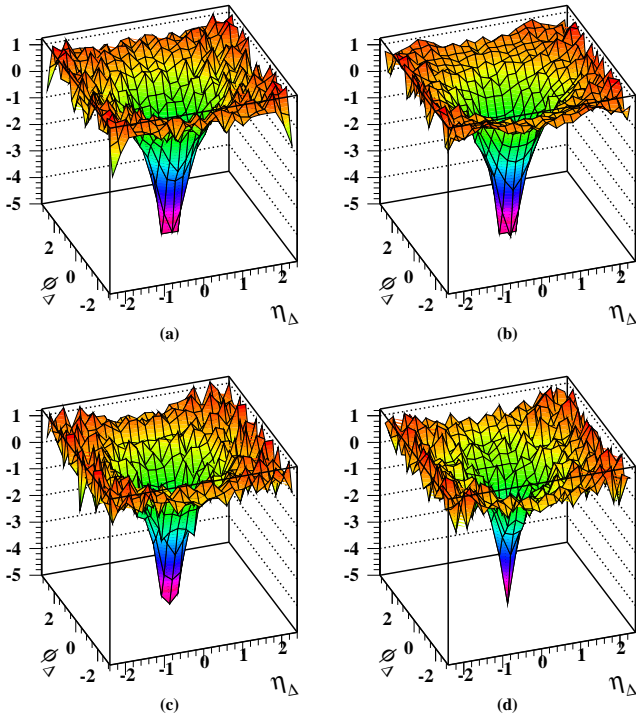


FIG. 2: Perspective views of two-particle CD joint autocorrelations $\bar{N}(\hat{r}-1)$ on $(\eta_\Delta, \phi_\Delta)$ for central (a) to peripheral (d) collisions. Center bins at $\phi_\Delta = \eta_\Delta = 0$, containing photon-conversion electron pairs, were omitted from model fits.

sions [7, 17], a conclusion which is however misleading. For A-A collisions a more complete picture is obtained from 2D joint autocorrelations on combined difference variables $(\eta_\Delta, \phi_\Delta)$, as shown in Fig. 2.

Invariance of correlation structure on sum variables $\eta_1 + \eta_2$ and $\phi_1 + \phi_2$ in Fig. 1 implies that those distributions can be projected onto their respective difference variables to form 1D *autocorrelation* distributions [10] *without loss of information*. If projections are implemented on both difference variables the resulting 2D *joint* autocorrelation on $(\eta_\Delta, \phi_\Delta)$ compactly represents *all* correlation information on momentum subspace $(\eta_1, \eta_2, \phi_1, \phi_2)$. Shown in Fig. 2 are perspective views of CD joint autocorrelations for four centrality classes. Quantity $\bar{N}(\hat{r}-1)$ [18] represents *per-particle* correlations and is $O(1)$ for all centralities. Fig. 2 distributions are dominated by a 2D negative peak: broader and elliptical for peripheral collisions with major axis along ϕ_Δ , transitioning smoothly to a narrower and deeper peak symmetric on $(\eta_\Delta, \phi_\Delta)$ for central collisions. The vertical axis limits were chosen to display large-scale structure. 1D projections of Fig. 2 distributions onto individual difference variables ϕ_Δ and η_Δ are shown in Fig. 3. Solid dots (open triangles) correspond to η_Δ (ϕ_Δ) projections.

Statistical errors for \hat{r} in Fig. 1 (central collisions) are ± 0.00015 for all bins. Statistical errors for 1D autocorrelations are uniform on ϕ_Δ (periodic variable) but approximately double as $|\eta_\Delta|$ increases from 0 to 2 (finite η accep-

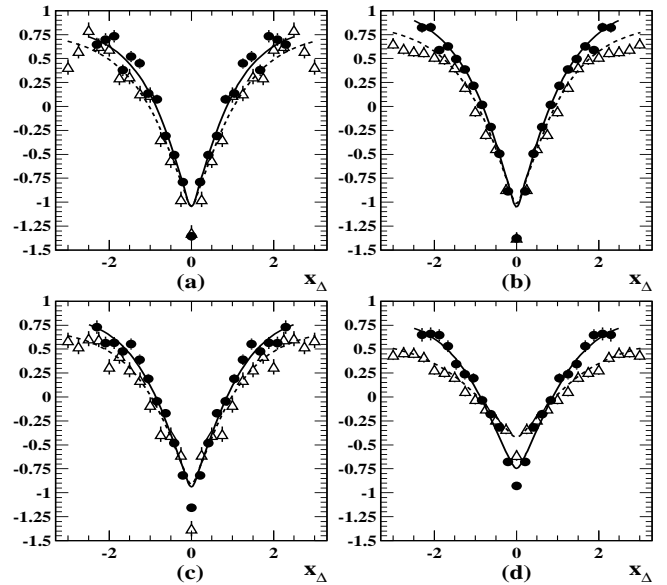


FIG. 3: Projections of 2D CD joint autocorrelations $\bar{N}(\hat{r}-1)$ in Fig. 2 onto individual difference variables η_Δ (solid points) and ϕ_Δ (open points) for central (a) to peripheral (d) collisions. Solid (dashed) curves represent corresponding projections of 2D analytical model fits to the data. 2D peaks are substantially reduced in amplitude by 1D projections.

tance). Statistical errors at $\eta_\Delta \sim 0$ vary from ± 0.00015 for central collisions to ± 0.0007 for peripheral collisions, again reflecting the $1/\bar{N}$ dilution factor. In contrast, statistical errors for $\bar{N}(\hat{r}-1)$ in Fig. 2 ($\pm 0.2 =$ one tick, for $\eta_\Delta \sim 0$) are independent of centrality. Statistical errors for projections in Fig. 3 are shown explicitly in that figure by error bars. Systematic errors were estimated as in [11]. The dominant systematic error is correlations from resonance (ρ^0, ω) decays, estimated to be about 10% of the peaks in Fig. 2 in the range $|\eta_\Delta| < 0.5, |\phi_\Delta| < 2$ [19].

Joint autocorrelations in Fig. 2 were fitted with a model function consisting of a 2D function peaked on both η_Δ and ϕ_Δ and a 1D gaussian on η_Δ (the latter motivated by the p-p limiting case [17, 20]) plus constant offset, all defined relative to quantity $\hat{r}-1$ as

$$F = A_0 + \sum_{k=1}^2 A_k e^{-\left[\left(\frac{\phi_\Delta}{\sqrt{2}\sigma_{\phi_\Delta, k}} \right)^2 + \left(\frac{\eta_\Delta}{\sqrt{2}\sigma_{\eta_\Delta, k}} \right)^2 \right] \frac{P_k}{2}}, \quad (2)$$

where $k=1$ corresponds to the 2D peak on $(\eta_\Delta, \phi_\Delta)$, and $k=2$ corresponds to the independent gaussian peak on η_Δ ($\sigma_{\phi_\Delta, 2} \rightarrow \infty$). $P_1 = 1$ represents the observed exponential shape of the 2D peak, while P_2 and $\sigma_{\eta_\Delta, 2}$ were fixed at 2 and 1.5 (parameter P controls peak shape). F interpolates between the 1D gaussian peak observed in p-p and the 2D exponential peak observed in central Au-Au collisions. Best-fit values for the varied parameters and χ^2/DoF for the four centralities are listed in Table I. Total systematic error for extrapolated quantities [21] in Table I was 11% (errors added in quadrature).

TABLE I: Parameters and fitting errors (only) for model fits [Eq. (2)] to joint autocorrelation data in Fig. 2 for centrality bins (a) - (d) (central - peripheral). Total systematic error for normalized amplitudes is 11%.

centrality	(d)	(c)	(b)	(a)	error ^a (%)
S	1.19	1.22	1.25	1.27	8 ^b
\bar{N}	115.5	424.9	789.3	983.0	
$S\bar{N}A_0$	0.98	0.80	0.91	0.79	11- 12
$S\bar{N}A_1$	-4.1	-6.8	-7.7	-7.7	6-4
$\sigma_{\phi_{\Delta},1}$	0.66	0.54	0.51	0.51	11-5
$\sigma_{\eta_{\Delta},1}$	0.46	0.42	0.41	0.41	10-5
$S\bar{N}A_2$	-0.51	-0.11	-0.15	-0.021	0.17-0.19 ^c
χ^2/DoF	$\frac{380}{315}$	$\frac{315}{315}$	$\frac{314}{315}$	$\frac{329}{315}$	

^aRange of fitting errors in percent from peripheral to central.

^bSystematic error.

^cMagnitude of fitting errors.

The model fits indicate that with increasing centrality the 2D peak exhibits 1) strong amplitude increase, 2) significant width reduction and 3) approach to approximately equal widths on ϕ_{Δ} and η_{Δ} for central collisions.

Charge-dependent correlations for central Au-Au collisions differ markedly from p-p data. CD correlations for p-p collisions are dominated by a 1D negative gaussian peak on η_{Δ} with $\sigma_{\eta_{\Delta}} \simeq 1$ [17, 20], associated with charge ordering on z during string fragmentation [7]. For the most peripheral Au-Au centrality in this analysis (d) we observe CD correlation structure intermediate between p-p and central Au-Au collisions. In the latter case a large-amplitude 2D negative exponential peak dominates the correlation structure, with similar widths on η_{Δ} and ϕ_{Δ} much reduced from p-p collisions. Variation of peak amplitudes and widths with Au-Au centrality are shown in Fig. 4, along with p-p limiting cases (bands and line) from STAR p-p data at 200 GeV [20] ($\nu = 1$), consistent with ISR p-p data at 52.5 GeV [17]. *Efficiency-corrected* per-particle amplitudes $-S\bar{N}A$ for central Au-Au collisions exceed those for p-p collisions by a factor 10, strongly contradicting a p-p linear superposition hypothesis [18].

These results suggest that CD correlations in Au-Au collisions, as in p-p collisions, derive from configuration-space charge ordering but that the hadronization geometry changes from 1D in p-p to 2+ dimensions in central Au-Au collisions, contributing to the peak symmetry on $(\eta_{\Delta}, \phi_{\Delta})$. In Fig. 4 the contribution from 1D charge ordering (gaussian peak on η_{Δ}) is already substantially reduced for centrality (d) ($\nu \sim 2.5$) in favor of the symmetric component. A hadron-opaque medium in central collisions may contribute to the newly-observed *exponential* peak shape. An exponential distribution on pair opening angle [radius on (η, ϕ)] is consistent with: 1) correlations detected only if both members of a correlated pair are not significantly scattered, 2) scattering probability measured by a mean free path, 3) mean path length in the medium increasing monotonically with pair opening angle. That picture assumes that CD correlations are not due to parton fragmentation outside the medium.

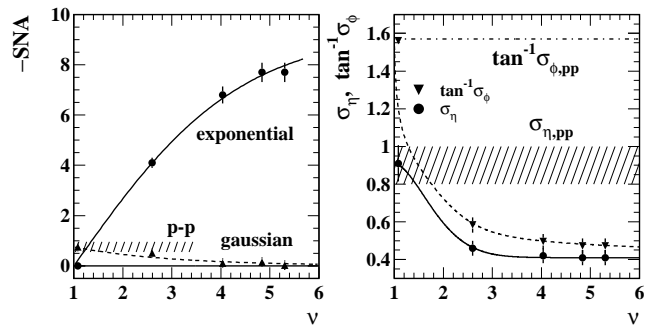


FIG. 4: Left panel: Amplitudes for exponential (dots) and gaussian (triangles) peak components from Table I for peaks in Fig. 2 are plotted on mean path length ν [16]. Right panel: Fitted widths $\sigma_{\eta_{\Delta}}$ (dots) and $\tan^{-1} \sigma_{\phi_{\Delta}}$ (triangles) are also plotted on ν . Hatched regions, dash-dot line and $\nu = 1$ data points summarize p-p limiting values. Curves guide the eye.

Contributions from charge ordering in jet fragmentation were sought by splitting central Au-Au data at $p_t = 0.5$ GeV/c, below which jet fragments should be negligible. Peak structures as in Fig. 2 dominated both subsamples, although the amplitudes were somewhat different.

HIJING [5] and RQMD [9] charge-dependent correlations qualitatively disagree with data. Hijing charge-dependent correlations are derived from the Lund model *via* Pythia, and are consequently consistent with p-p 1D string fragmentation for all A-A centralities: a 1D gaussian on η_{Δ} with amplitude about 10% of the peak in Fig. 2 (a). RQMD, dominated by resonance decays and hadronic rescattering, exhibits a broad 2D gaussian on $(\eta_{\Delta}, \phi_{\Delta})$, with amplitude also about 10% of data for central collisions. Large-scale correlations as in Fig. 1 observed for US *and* LS pairs in data are consistent with local charge ordering but inconsistent with CD correlations from decays of hadronic resonances such as the ρ^0 , which would affect only the US pair type, further arguing against a resonance-gas scenario.

In summary, we have measured charge-dependent joint autocorrelations on difference variables ϕ_{Δ} and η_{Δ} for Au-Au collisions at $\sqrt{s_{NN}} = 130$ GeV. The data are consistent with local charge conservation or canonical suppression of net charge fluctuations, evolving from 1D color-string fragmentation in p-p collisions to exponentially-attenuated 2D charge-ordered emission from a hadron-opaque medium in central Au-Au collisions. These results are qualitatively inconsistent with standard collision models. Charge-dependent autocorrelations provide unique access to the geometry of hadronization and rescattering as the energy density and spatial extent of A-A collisions increase with centrality.

We thank the RHIC Operations Group and RCF at BNL, and the NERSC Center at LBNL for their support. This work was supported in part by the HENP Divisions of the Office of Science of the U.S. DOE; the U.S. NSF; the BMBF of Germany; IN2P3, RA, RPL, and EMN of France; EPSRC of the United Kingdom;

FAPESP of Brazil; the Russian Ministry of Science and Technology; the Ministry of Education and the NNSFC of China; Grant Agency of the Czech Republic, FOM

and UU of the Netherlands, DAE, DST, and CSIR of the Government of India; Swiss NSF; and the Polish State Committee for Scientific Research.

-
- [1] R. Stock, Nucl. Phys. **A661**, 282 (1999); H. Heiselberg, Phys. Rep. **351**, 161 (2001).
- [2] A. Dumitru, R. Pisarski, Phys. Lett. **B504**, 282 (2001).
- [3] L. M. Bettencourt, K. Rajagopal and J. V. Steele, Nucl. Phys. **A693**, 825 (2001).
- [4] M. Gaździcki, A. Leonidov, G. Roland, Eur. Phys. J. **C6**, 365 (1999).
- [5] X.N. Wang, M. Gyulassy, Phys. Rev. D **44**, 3501 (1991).
- [6] Q. Liu and T. A. Trainor, Phys. Lett. **B567**, 184 (2003).
- [7] B. Andersson, G. Gustafson, G. Ingelman and T. Sjöstrand, Phys. Rep. **97**, 31-145 (1983).
- [8] M. Asakawa, U. Heinz, B. Müller, Phys. Rev. Lett. **85**, 2072 (2000); S. Jeon, V. Koch, Phys. Rev. Lett. **85**, 2076 (2000).
- [9] H. Sorge, H. Stöcker, W. Greiner, Nucl. Phys. **A498**, 567c (1989); Ann. Phys. (N.Y.) **192**, 266 (1989).
- [10] An autocorrelation is a projection by averaging of a distribution on (x_1, x_2) onto difference variable $x_1 - x_2$.
- [11] J. Adams *et al.* (STAR Collaboration), eprint nucl-ex/0308033.
- [12] K. H. Ackermann *et al.*, Nucl. Instrum. Meth. A **499**, 624 (2003); see other STAR papers in volume **A499**.
- [13] C. Adler *et al.*, Phys. Rev. Lett. **87**, 112303 (2001); *ibid.* **89**, 202301 (2002).
- [14] C. Adler *et al.* Phys. Rev. Lett. **87**, 082301 (2001).
- [15] Centrality classes d) - a) respectively were defined by N/N_0 [16] cuts at > 0.03 , 0.21 , 0.56 and > 0.79 .
- [16] Quantity $\nu \simeq 5.5 (N_{part}/N_{part,max})^{1/3} \simeq 5.5 (N/N_0)^{1/3}$ estimates mean participant path length as a number of encountered nucleons. N_0 is the half-maximum end point of the minimum-bias distribution plotted as $d\sigma/dN_{ch}^{1/4}$.
- [17] D. Drijard *et al.* (ACCDHW Collaboration), Nucl. Phys. B **166**, 233 (1980).
- [18] $\bar{N}(\hat{r} - 1)$, measuring *per-particle* correlations (typically $O(1)$ for all centralities), is *invariant* with centrality if A-A collisions are linear superpositions of p-p collisions.
- [19] R. Ray and R. Longacre, nucl-ex/0008009, unpublished.
- [20] R. J. Porter and T. A. Trainor (STAR Collaboration), eprint hep-ph/0406330
- [21] Extrapolation factors \mathcal{S} for $\bar{N}A_k$ provide corrections for background contamination and tracking inefficiency [13]. Systematic error in \mathcal{S} was estimated to be $\pm 8\%$.